A PARAMETERIZED SIMULATION OF DOPPLER LIDAR

by

David B. Chester

A thesis submitted in partial fulfillment
of the requirements for the degree

of

MASTER OF SCIENCE

in

Electrical Engineering

Approved:

_____   _____
Scott E. Budge, PhD   Jacob Gunther, PhD
Major Professor   Committee Member

_____   _____
Charles M. Swenson, PhD   Mark R. McLellan, PhD
Committee Member   Vice President for Research and
                                         Dean of the School of Graduate Studies

UTAH STATE UNIVERSITY
Logan, Utah

2017

CONTENTS

LIST OF FIGURES

CHAPTER 1

Introduction

1.1 Overview

Recent and upcoming missions for the exploration of solar system bodies require accurate position and velocity data during the descent phase to ensure safe landing at predesignated sites. Because of inertial measurement unit (IMU) drift during travel, the data provided by the IMU may not be reliable. One solution proposed by NASA is the use of a frequency modulated continuous wave (FMCW) Doppler lidar system during the landing phase to provide additional information about attitude, position, and velocity to contribute to a successful landing [7–9]. The optimization and comparison of potential configurations of such a system would be greatly aided by an appropriate simulation tool.

LadarSIM is a robust parametrized simulation tool for time of flight lidar developed at Utah State University's Center for Advanced Imaging Ladar over the past decade and a half [1, 2]. LadarSIM has the flexibility to simulate a wide range of time of flight lidar systems with varying beam and scanner patterns as well as parametrized transmitters and receivers. These simulated systems can be evaluated using scenarios consisting of user specified terrain, targets, and flight paths.

The research for this thesis had three objectives. First, to add a parameterized simulation of an FMCW lidar transmitter and receiver, second, to utilize that simulation to perform a trade-off study to determine the effects of varying laser transmission power, beam divergence, aperture diameter, and FFT size on a Doppler lidar system, and third, to use the simulation to compare traditional and novel scanning patterns in planetary landing scenarios.

The simulation developed for this thesis is a useful tool for the development of Doppler lidar systems with a wide range of transceiver characteristics and nearly arbitrary beam

and scanning parameters. The information gained from the trade-off study will provide valuable insight for someone designing or selecting a Doppler lidar system to meet mission requirements. The point clouds generated in the exploration of novel scanning patterns give an idea of the potential utility of a Doppler lidar system for terrain mapping, navigation, and hazard avoidance.

1.2   Chapter Outlines

This thesis will describe the theory of FMCW lidar, how LadarSIM was expanded to add a simulation of Doppler lidar, and present results from LadarSIM's Doppler lidar simulation. To achieve this the thesis will be structured as follows. Chapter 2 will describe the theory behind FMCW radar detection and show how the same basic concepts can be applied to a lidar system. Chapter 3 will present some background information on LadarSIM and then show how it was modified to include a simulation of Doppler lidar. Chapter 4 will present a trade-off study exploring the effects of laser transmission power, beam divergence, aperture diameter, and FFT size on a Doppler lidar system. Chapter 5 will discuss novel scanning patterns and present point clouds generated by LadarSIM for those patterns. Chapter 6 is the conclusion of the thesis and will also discuss the potential for future work.

CHAPTER 2

Frequency Modulated Continuous Wave Detection

2.1 FMCW Radar

The theory behind Frequency Modulated Continuous Wave (FMCW) detection will be explored in this section following the development of Brooker [3]. Booker's development focuses on FMCW radar, but the same theory applies to FMCW lidar by making the appropriate changes in the system hardware. For example, the antennae would be replaced with a telescope etc.

2.1.1 Basic Principles

FMCW detection refers to a radar/lidar system in which a continuous wave of known frequency is modulated in amplitude, transmitted, and the reflected signal is detected. A continuous wave radar in which a single microwave oscillator serves as both the transmitter and local oscillator (LO) is, generally speaking, a homodyne radar. Frequency modulated continuous waveform (FMCW) radar systems often leverage a homodyne architecture.

An FMCW radar uses a continuous wave signal which is modulated in amplitude over a range of frequencies creating a linear chirp. This chirped signal is radiated to the target and an echo returns after time T_p, which is the time it takes for the signal to reach the target and reflected energy to return to the antennae. Figure 2.1 illustrates a chirped signal, shown with a solid line, and the return signal delayed by T_p, shown with a dashed line. In this figure f_b refers to the difference in frequency of the two signals at a given time.

It is clear that the distance to the target can be calculated with T_p. In an FMCW system T_p is determined by measuring the beat frequency f_b. To do this a portion of the signal produced by the LO is mixed with the returned echo producing f_b. A signal chirped
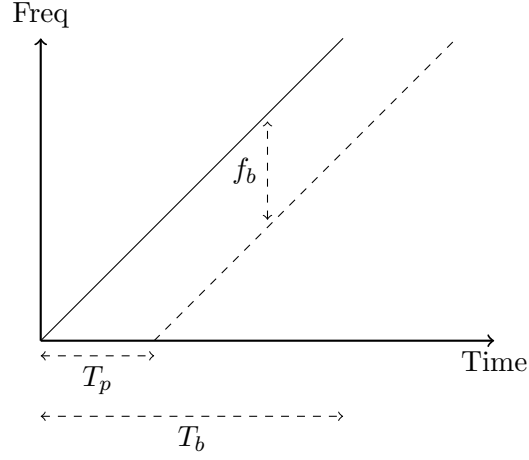
Fig. 2.1: Transmit and Receive Doppler Shift

in frequency can be expressed as

$$v_{fm}(t) = A_c cos[\omega_c t + \frac{A_b}{2}t^2].$$ (2.1)

Where A_b is a constant of proportionality between the change in frequency over the chirp or chirp slope, ω_b, and the chirp time; such that $\omega_b = A_b t$. The mixture of the transmitted and received signals can be expressed as

$$v_{fm}(t - T_p)v_{fm}(t) = A_c^2 cos[\omega_c t + \frac{A_b}{2}t^2]cos[\omega_c(t - T_p) + \frac{A_b}{2}(t - T_p)^2].$$ (2.2)

This simplifies to

$$v_{out}(t) = A_c^2(cos[(2\omega_c - A_b T_p)t + A_b t^2 + (\frac{A_b}{2}T_p^2 - \omega_c T_p)] + cos[A_b T_p t + (\omega_c T_p - \frac{A_b}{2}T_p^2)]).$$ (2.3)

It is desirable to isolate the second term in Eq 2.3 because it is the the beat signal. The first cosine term is an FM chirp at about twice the carrier frequency and is in most cases conveniently filtered out because it is above the cutoff frequency of the receiver components.

To obtain the f_b from the beat signal the phase term is differentiated with time,

$$f_b = \frac{1}{2\pi} \frac{d}{dt}[A_b T_b t + (\omega_c T_p - \frac{A_b}{2}T_p^2)], \tag{2.4}$$

resulting in

$$f_b = (\frac{A_b}{2\pi})T_p. \tag{2.5}$$

2.1.2   FMCW Detection

As discussed above, the most common way to obtain the beat frequency, f_b, is to take the product of the transmitted chirp signal and the received signal and filter to isolate the constant frequency beat. The Fast Fourier Transform (FFT) is the most common method of spectral analysis employed in FMCW radar to measure f_b.

Given a chirp duration, T_b(s), and assuming that $T_b \gg T_p$, the maximum resolution of the beat frequency is $2/T_b$(Hz). Figure 2.1 shows a chirp which meets that criterion. The resolution bandwidth of a signal, δf_b, is commonly defined between its 3 dB points. For the truncated chirp case δf_b coincides with a region of width $1/T_b$ centered on f_b, as shown in figure 2.2.

The chirp bandwidth is the total change in frequency for the chirp, Δf. Clearly the slope of the chirp is the chirp bandwidth divided by the chirp time, $\Delta f/T_b$. Eq 2.5 can then be restated

$$f_b = (\frac{A_b}{2\pi})T_p = \frac{\Delta f}{T_b}T_p. \tag{2.6}$$

Intuitively T_p is the round trip time from the antennae to the target and back

$$T_p = 2\frac{2R}{c}, \tag{2.7}$$

where c is the speed of light. The classical FMCW formula is obtained by substituting into eq 2.6:

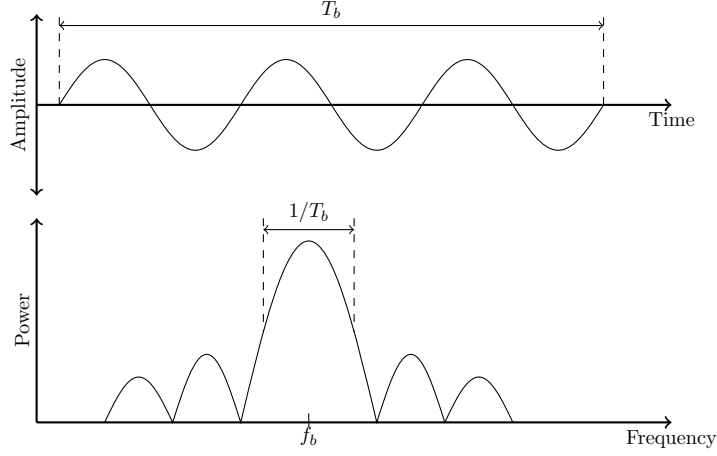$$f_b = \frac{\Delta f}{T_b}\frac{2R}{c}, \tag{2.8}$$

Fig. 2.2: Spectrum of the truncated sinusoidal signal output by an FMCW radar.

relating the beat frequency to the range. Solving for range yields

$$R = \frac{T_b c}{2\Delta f} f_b. \tag{2.9}$$

Eq 2.9 relates range to beat frequency. The same equation can be used to related range resolution δf and chirp bandwidth:

$$\delta R = \frac{T_b c}{2\Delta f} \delta f = \frac{c}{2\Delta f}. \tag{2.10}$$

Where the frequency resolution $delta f$ is approximately equal to $1/T_b$.

2.1.3   Doppler Effect in FMCW

So far the development in this section has assumed a stationary radar and target. The case where the radar, the target, or both are moving will now be examined. The Doppler effect describes the change in observed and transmitted frequencies when the distance between the two is changing. The relationship between the transmitted frequency, f_c, and the received frequency, f_r can be expressed

$$f_r = \frac{c + v_t}{c + v_s} f_c. \tag{2.11}$$

Where v_t is the velocity of the target and v_s is the velocity of the source. From eq 2.11 it is simple to obtain an equation for the change in frequency, Δf in relation to the difference in velocity of the source and target, Δv:

$$\Delta f = \frac{\Delta v}{c} f_s. \tag{2.12}$$

For the following development the radial velocity, $v_r(\text{m/s})$, will represent the velocity term causing the Doppler effect. Modifying eq 2.1 to incorporate the Doppler shift of the echo signal yields:

$$v_{fm}(t - T_p) = A_c cos[\omega_c(t - T_p) + \frac{A_b}{2}(t - T_p)^2 - \frac{2v_r}{c}\omega_c(t - T_p)]. \tag{2.13}$$

The new beat frequency then is the same as derived in eqs 2.5 and 2.6 shifted by the Doppler frequency, f_d:

$$f_b = \frac{2v_r}{c}f_c - \frac{A_b}{2\pi}T_p = f_d - \frac{A_b}{2\pi}T_p. \tag{2.14}$$

For a chirp with positive A_b, an up-chirp, the beat frequency will be the difference between the Doppler frequency f_d and the beat frequency caused by the echo time or range frequency f_r. For a down-chirp, a negative slope, the beat frequency will be the sum of the Doppler frequency and the range frequency. In many radar applications it can be assumed that the Doppler frequency is lower than the range frequency leading to eqs 2.15 and 2.16. If f_d ¿ f_b, as is frequently the case in Lidar, the roles of f_d and f_b are reversed.

$$f_{bUp} = f_b - f_d \tag{2.15}$$

$$f_{bDown} = f_b + f_d \tag{2.16}$$

By using a triangle waveform the sum and difference frequencies can be obtained to isolated range and velocity measurements. Fig 2.3 illustrates the Doppler effect on an FMCW waveform transmitting a triangle wave pattern. Expressions for f_r and f_d can be

obtained by averaging and differencing eqs 2.15 and 2.16:

$$f_r = \frac{f_{b(Up)} - f_{b(Down)}}{2},$$ (2.17)

$$f_d = \frac{f_{b(Up)} + f_{b(Down)}}{2}.$$ (2.18)

The sign of f_d is determined by the direction of motion. If the range is getting smaller f_d will be positive and if the range is getting larger f_d will be negative.

2.2 FMCW Lidar Processing

The two main differences between FMCW lidar and radar are the modulation frequencies and the wavelength of the radiation. One consequence of this is that the doppler frequency is usually higher than the beat frequency, leading to some minor modifications to the equations in section 2.1. The most importantly the relationship between beat frequency of the up-chirp with the doppler frequency is better expressed as:

$$f_{bUp} = f_d - f_b.$$ (2.19)

In a practical FMCW lidar system it is common to add a period of constant frequency between up and down chirps in the chirp process illustrated in figures 2.3. Doing this gives a direct measurement of the Doppler frequency. This modified chirp process is shown in figure 2.4.

From the process process illustrated in figure 2.4 the system obtains three measured frequencies: $f_{b(Up)}$ the up-chirp frequency, f_d the Doppler frequency, and $f_{b(Down)}$ the down-chirp frequency. The range information is encoded in the beat frequency f_r which is obtained from $f_{b(Up)}$ and $f_{b(Down)}$ by eq 2.17, substituting this result into 2.9 yields:

$$R = \frac{T_b c}{2B} \frac{f_{b(Up)} - f_{b(Down)}}{2}.$$ (2.20)

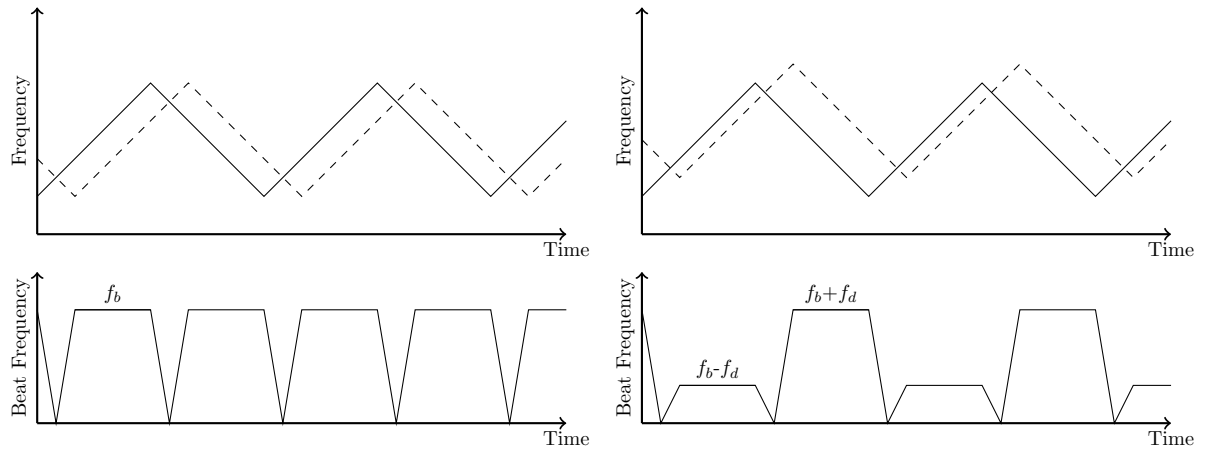Where B is the chirp bandwidth. Similarly the velocity measurement can be obtained
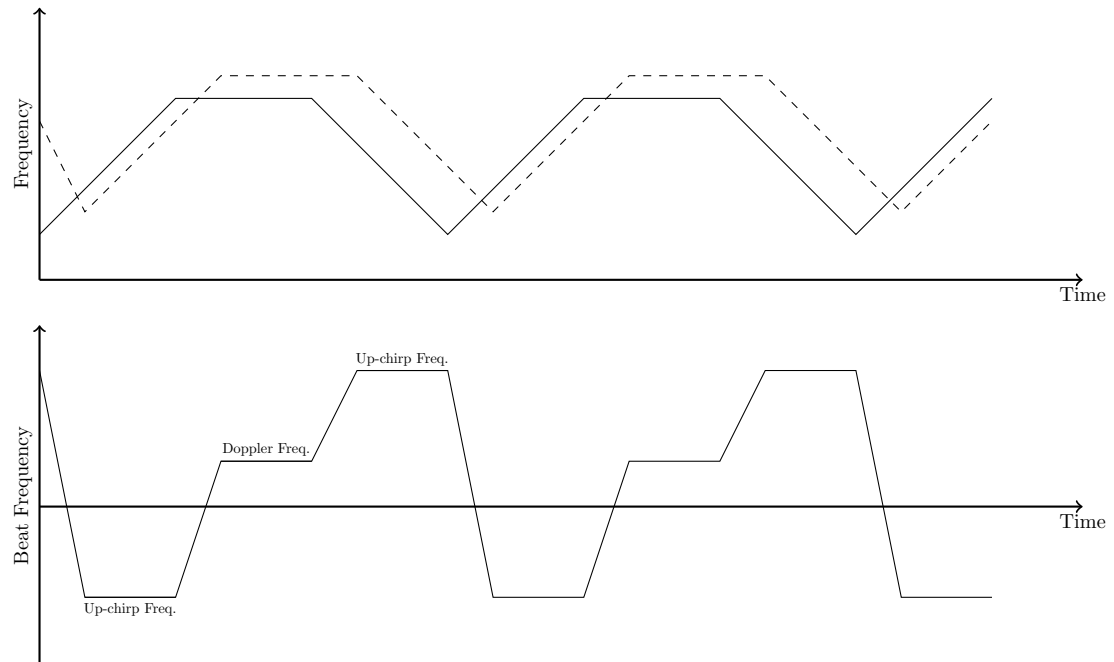
Fig. 2.3: Doppler Effect on FMCW radar.

Fig. 2.4: Doppler Effect on FMCW lidar with up-chirp, steady, and down-chirp sections.

using the three available frequencies. One option is to use the measured Doppler frequency directly by substituting into eq 2.12 and solving for the velocity. The problem here is that the sign of f_d determines the direction of motion and the sign of f_d is not preserved in the FFT process. A better option is to use 2.18 to get f_d and plug the result into 2.12 and solve for velocity resulting in:

$$V = \frac{\lambda}{2} \frac{f_{b(Up)} + f_{b(Down)}}{2}. \tag{2.21}$$

2.3 FMCW Lidar Architecture

The above section explored the basic functionality of FMCW radar then showed which changes must be made to the equations for detection. In this section a number of detection architectures for FMCW lidar will be examined. Adany et al. provide and analysis of direct detection, heterodyne detection, as well as their proposed simplified homodyne detection [4,5], which will serve as the primary source of information in this section.

2.3.1 Direct Detection Architecture

In an FMCW direct detection scheme, the signal from the modulation waveform generator is split. Part of the signal is used to modulate the amplitude of the laser, which is then amplified and sent to the telescope. The returning light is captured through the same telescope and converted into an electrical signal via a photo detector. The other part of the modulation signal is then mixed with the electrical signal from the detected returning light to perform de-chirping. An FFT is then taken on the de-chirped signal to find the beat frequency and the range information. The returning signal is weak so the signal to noise ratio (SNR) at the output of the photodiode is primarily limited by thermal noise. Considering only thermal noise leads to the following expression for the maximum SNR:

$$SNR_{dir} \approx \frac{2\Re^2 P_{sig}^2}{\frac{4kTB_e}{R_L}}. \tag{2.22}$$

Where $\Re$ is the photodiode responsivity, P_{sig} is the optical power of the received sigal,

k is Planck's constant, T is the absolute temperature, B_e is the electrical bandwidth, and R_L is the load resistance. Analysis of eq 2.22 shows that for every dB reduction in the return signal power the SNR is reduced by 2 dB. This disadvantage leads to very quick degradation of the performance of a lidar system using direct detection as range increases.
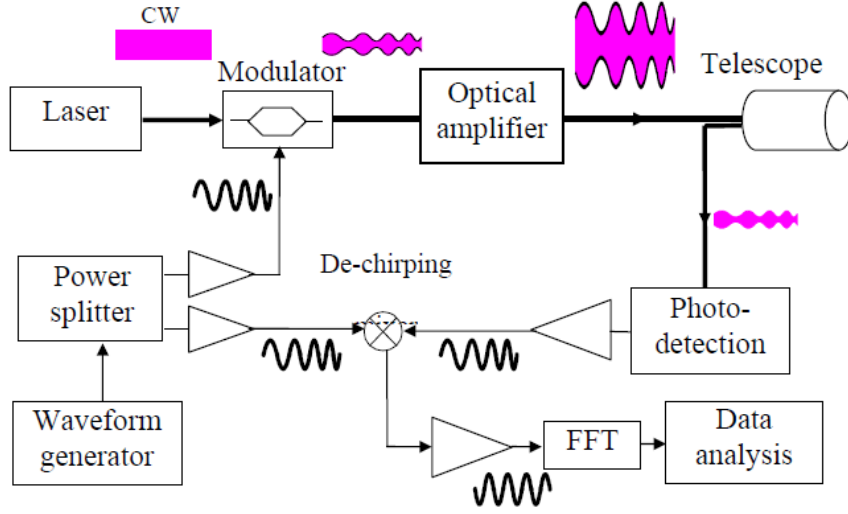

Fig. 2.5: Direct detection architecture

2.3.2 Coherent Heterodyne Detection Architecture

In coherent heterodyne detection the laser is split into two signals. One of these signals is modulated by the chirp waveform sent through an optical amplifier and out of the telescope. The other part of the the laser beam is used as the optical local oscillator. This LO signal is then shifted by an acousto-optic modulator to serve as the intermediate frequency (IF) for coherent heterodyne detection. The IF is optically mixed with the returning signal from the telescope, the output of the optical mixer is fed into a balanced photodiode. The photodiode rejects the direct detection component. The output of the photodiode is filtered to isolate the heterdyne IF signal which is detected by an envelope detector. The IF signal is then mixed with the modulation waveform for dechirping. An FFT is then performed on the dechirped signal to recover the beat frequency.

Optically mixing the returned signal with the LO helps mitigate the thermal noise in the photodiode. But because the strong optical LO, the SNR is limited by the shot noise. The theoretical best SNR for a coherent heterodyne lidar is

$$SNR_{het} \approx \frac{\Re P_{sig}}{2qB_e}.$$ (2.23)

In this equation q is the electron charge. In coherent heterodyne detection the SNR is linearly proportional to the optical power, making it more suitable for low power operation. The most significant disadvantage of coherent heterodyne detection is its complexity. The IF must be set much higher than the baseband, often in the GHz. This necessitates high speed optical detection and radio frequency (RF) processing circuitry. The IF envelope detection process mixes the signal with RF noise which can further limit the SNR. Because of this the theoretical SNR defined in eq 2.23 has not been obtained in a coherent heterodyne implementation [6].
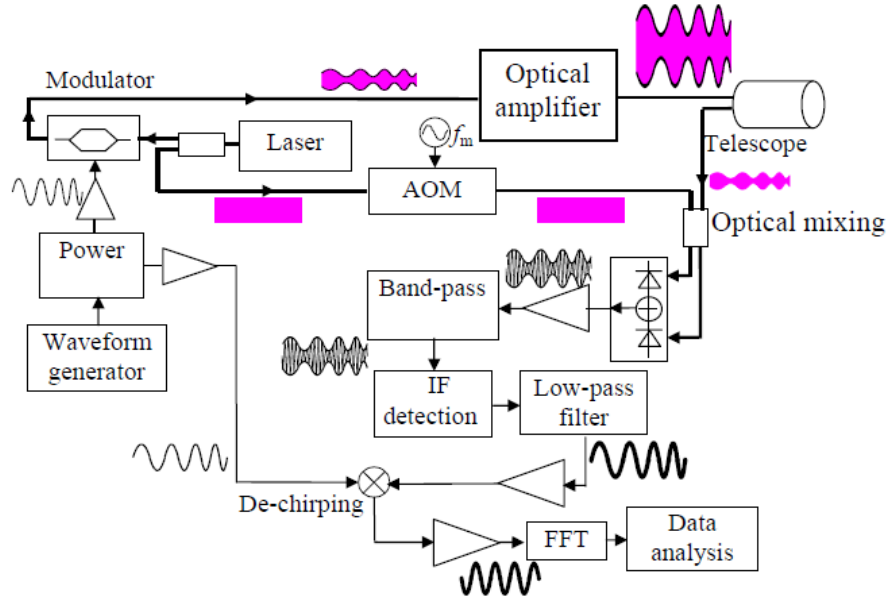

Fig. 2.6: Coherent heterodyne detection architecture

2.3.3   Homodyne Self-Chirped Detection Architecture

The homodyne self-chirped architecture was developed to maintain the receiver sensitivity obtained from coherent heterodyne detection while minimizing complexity. In this simplified homodyne detection scheme the laser is modulated by the chirp waveform then split in two. One part of the modulated laser is amplified and sent out the telescope, the other is used as the LO. The returned laser signal is mixed with the LO via a 2x2 optical coupler the output of which is fed into a balanced photodetector. Because the LO is modulated with the same waveform as the transmitted laser, the optical mixing performs both optical detection and RF de-chirping. This reduces the amount of RF noise which is introduced to the detection signal. Performing an FFT on the output of the photodetector yields the beat frequency.

The simplification of the signal path in the homodyne self-chirped architecture results in a practical SNR closer to the theoretical SNR in eq 2.23 than the practical SNR of the coherent heterodyne architecture.
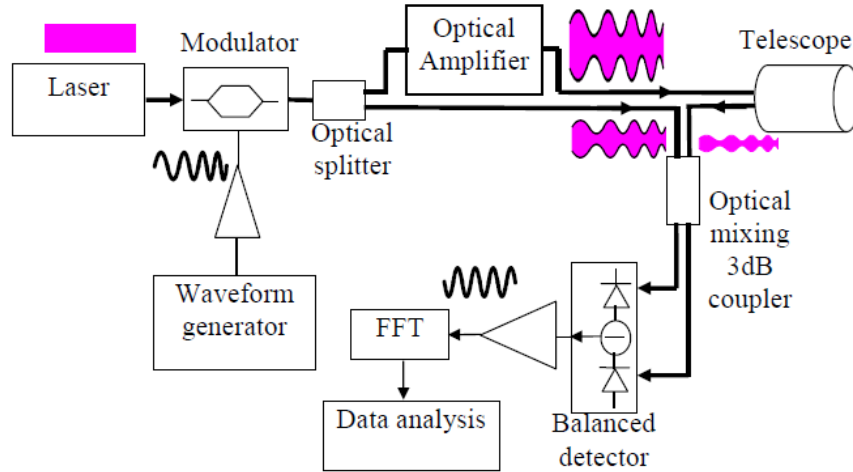

Fig. 2.7: Homodyne self-chirped detection architecture

This architecture is popular for its performance and simplicity. Because it is being

used by NASA for planetary landing missions [7–12], it has been selected as the basis for the simulation being reported on in this thesis.

CHAPTER 3

LadarSIM Modification

3.1 LadarSIM Background

LadarSIM is a robust parameterized tool for simulating lidar systems, which has been developed at Utah State University's Center for Advanced Imaging Ladar (CAIL) since 2003 [1, 2]. LadarSIM was originally developed to simulated pulsed time-of-flight lidar systems and has the flexibility to simulate a wide range of these systems by simulating parameterized lidar transceiver, focal plane arrays, and pointing/scanning systems, as well as the interaction of the lidar with a simulated 3D scene.

The main LadarSIM GUI is shown in figure 3.1. The GUI is split into three basic sections. In brown colored section in the center controls basic simulation parameters, such as scene selection, simulation fidelity, and what files the simulation will save.
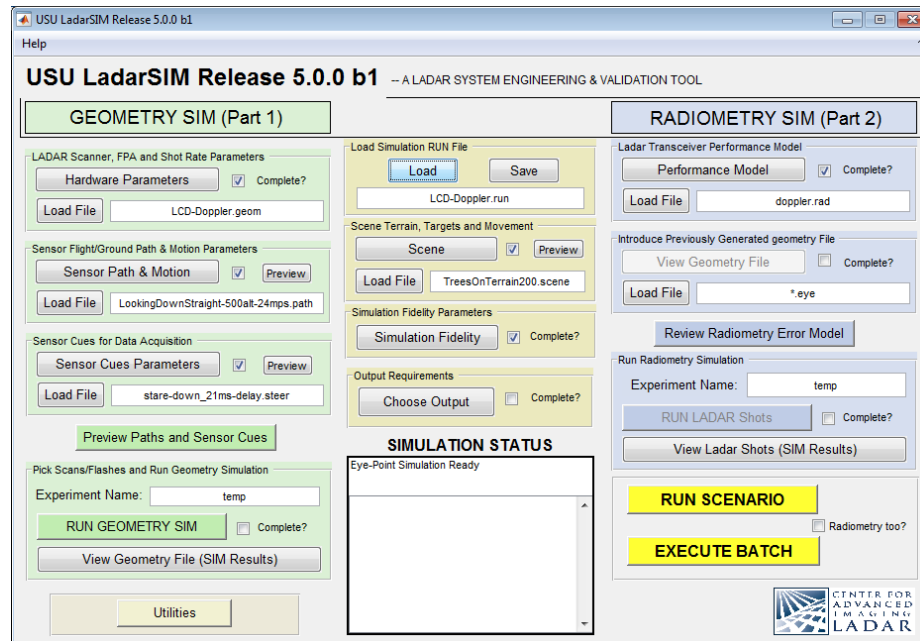

Fig. 3.1: Main GUI for running LadarSIM.

The green section on the left side of the GUI is the geometry simulation. This section simulates the scenario from a strictly geometric stand point. This simulation produces a point cloud using the scanner parameters, sensor flight path, and scene. The geometric simulation runs independently of the type of lidar to be simulated. The geometric measurements generated by the geometry simulation are used when LadarSIM simulates the actual performance of the specified lidar system.

The blue section on the right side of the GUI is the radiometric simulation. Again this cannot be run until after a geometric simulation of the scenario has been run. This side of the of the GUI can be used to simulate the performance of a particular lidar configuration. Parameters relating to the optical efficiency, transmitted beam, receiver, and range processing can be customized. The purpose of separating the geometric and radiometric simulations is that the output of a single geometric simulation can be used to evaluate the performance of different lidar configurations.

3.2   Geometry Simulation Modification

The geometry simulation produces two useful items. The first is a point cloud of the scenario based only on the flight path, scanning parameters, and the scene. The second is what is called the "eyepoint file." This file contains measurements of the true range for each instance that the lidar would take a measurement based on the scanning parameters. This file can be saved for later use or passed directly to the radiometry simulation.

Before a simulation of Doppler lidar was added to LadarSIM only time of flight (TOF) lidar was supported. In time of flight lidar no direct measurement of velocity is taken so it was not necessary to include true measurements of radial velocity. The measure of radial velocity is, however, crucial to the simulation of a Doppler lidar system. For this reason the geometry simulation was modified to add radial velocity measurements to the eyepoint file.

3.3   Radiometry Simulation Modification

Because the transmit and receive processes are very different for TOF and FMCW lidar, more modification was necessary to the simulation of the radiometry simulation.

Figure 3.2 shows the "performance model" window. This is where parameters pertaining to the radiometry simulation are set. LadarSIM divides these parameters into four sections, optics, transmitter, receiver, and range processing. The parameters in these subcategories are different for TOF and FMCW lidar, the radio button pair marked "Instrument Type" selects which type of system to be customized.
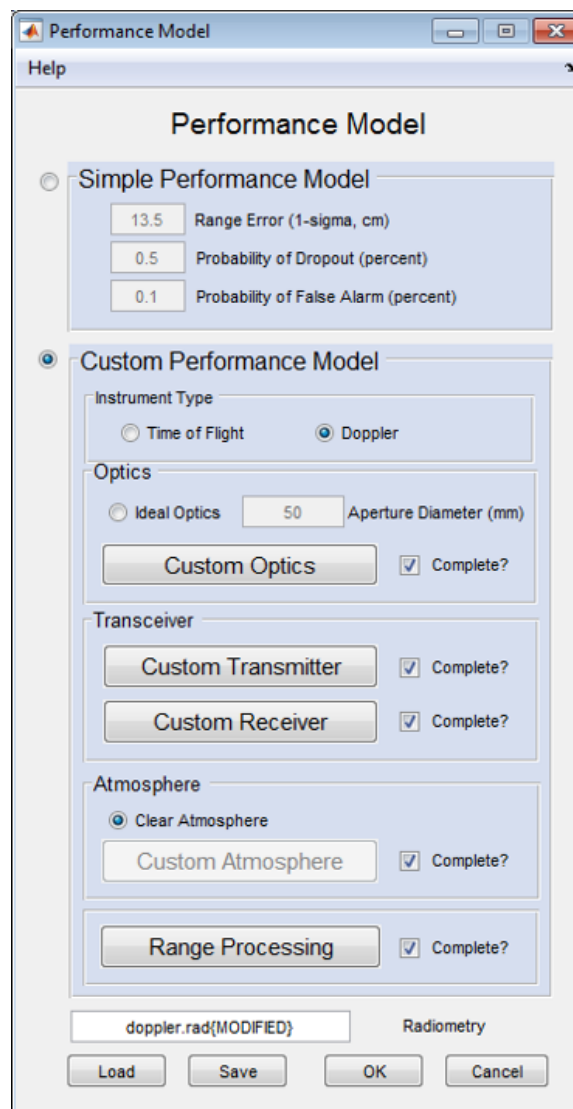

Fig. 3.2: Radiometry parameter GUI.

The Custom Optics GUI shown in figure 3.3 allows the user to specify the optical

efficiency of the transmitter and receiver, the aperture diameter, and detector fill factor. These parameters are common between TOF and FMCW lidar so this GUI is used for both.
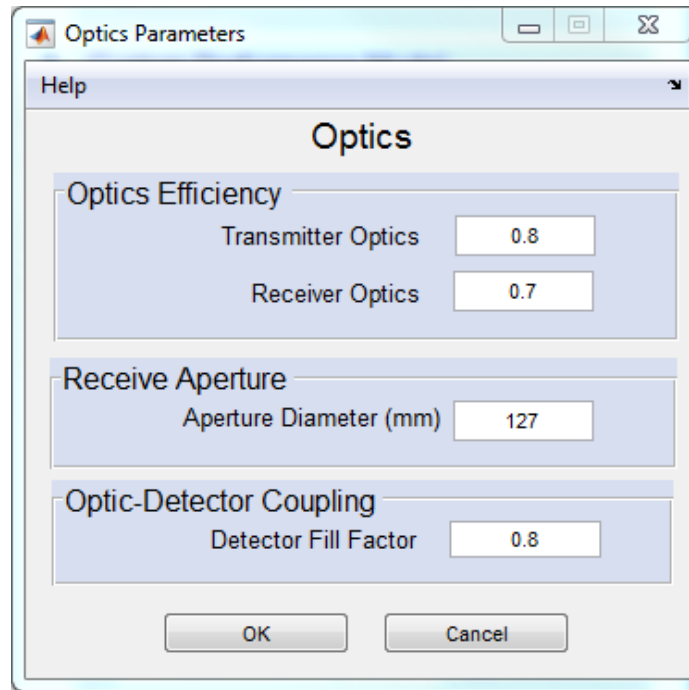
Fig. 3.3: Optical parameters GUI.

The Doppler Transmitter GUI is shown in figure 3.4. The user can use this GUI to set parameters related to the transmitted laser. Beam divergence, laser wavelength, and laser line width are important characteristics of the laser that have a large effect on the performance of the system. The "Temporal Pulse Shape" box allows users to specify the laser power and the chirp shape, which has a direct effect on the capabilities of the system. Chirp bandwidth length in time have a direct impact on the maximum resolution the system will be capable of.

The "Receiver Parameters" GUI can be used to describe the electronics of the receiver. The behavior of the photo-diode is important because it's bandwidth is leveraged in the directly by the homodyne self-chirped detection architecture discussed in section 2.3.3. The
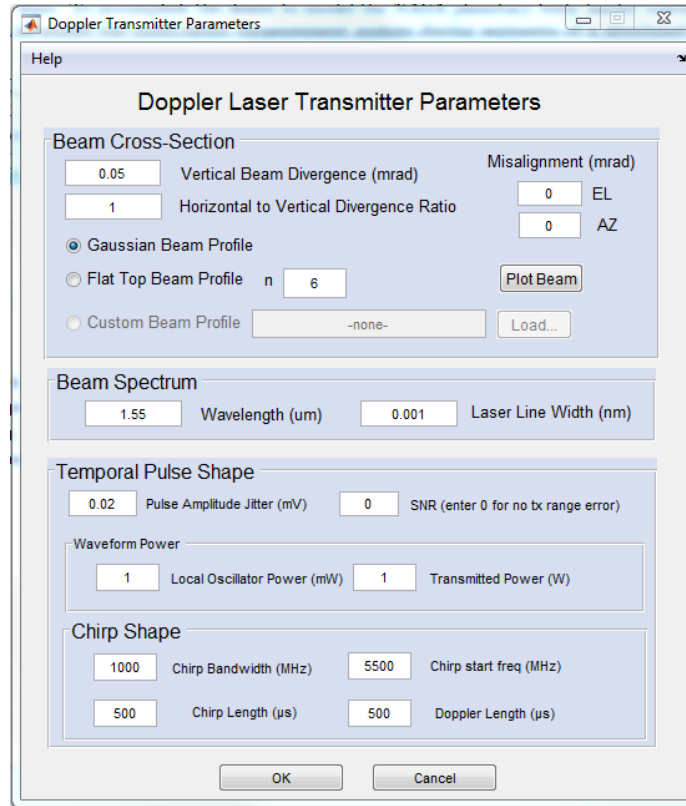
Fig. 3.4: Transmitter parameters GUI.

gain and bandwidth of other analog receiver electronics can also be specified in this GUI.

Parameters directly related to range processing are set in the "Doppler Range Processing" GUI shown in figure 3.2. The threshold to noise ratio (TNR) dictates where the detection threshold should be set in relation to the noise and effects the probability of detection and false alarm. The maximum range and Doppler velocity the system is capable of resolving is dependent on the sample rate. The user can select to specify either the maximum
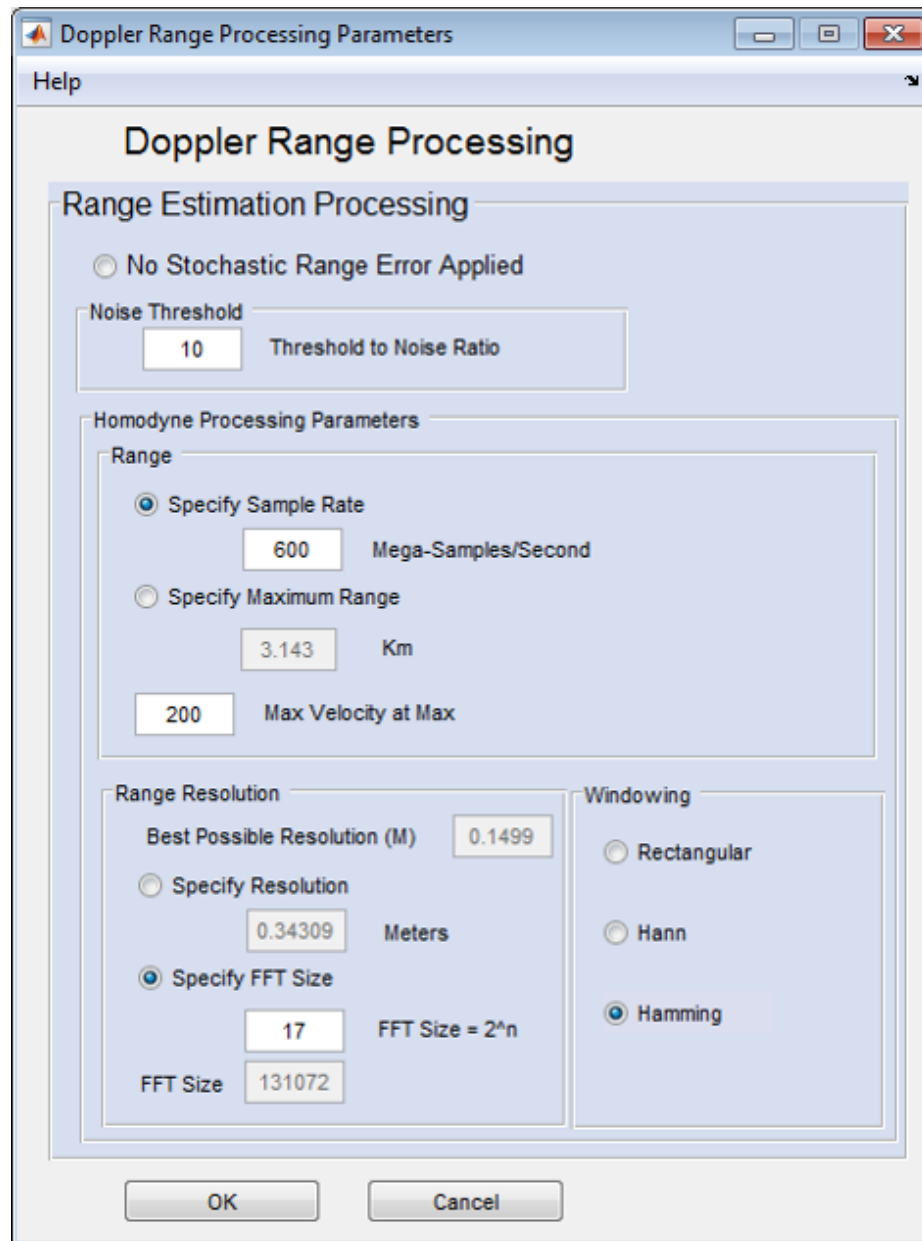
Fig. 3.5: Receiver parameters GUI.

Fig. 3.6: Range processing parameters GUI.

REFERENCES

[1] S. Budge, B. Leishman, and R. Pack, "Simulation and modeling of return waveforms from a ladar beam footprint in usu ladarsim," pp. 62 140N–62 140N–10, 2006. [Online]. Available: http://dx.doi.org/10.1117/12.666404

[2] K. D. Neilsen, S. E. Budge, R. T. Pack, R. R. Fullmer, and T. D. Cook, "Design and validation of the eyesafe ladar testbed (elt) using the ladarsim system simulator," pp. 73 230B–73 230B–7, 2009. [Online]. Available: http://dx.doi.org/10.1117/12.818856

[3] G. Brooker, "Introduction to sensors for ranging and imaging," 2009.

[4] P. Adany, C. Allen, and R. Hui, "Chirped lidar using simplified homodyne detection," *Journal of Lightwave Technology*, vol. 27, no. 16, pp. 3351–3357, Aug 2009.

[5] P. Adany, *Simplified homodyne detection for FM chirped lidar.* ProQuest, 2007.

[6] C. Allen, Y. Cobanoglu, S. K. Chong, and S. Gogineni, "Performance of a 1319 nm laser radar using rf pulse compression," in *IGARSS 2001. Scanning the Present and Resolving the Future. Proceedings. IEEE 2001 International Geoscience and Remote Sensing Symposium (Cat. No.01CH37217)*, vol. 3, 2001, pp. 997–999 vol.3.

[7] F. Amzajerdian, L. Petway, G. Hines, B. Barnes, D. Pierrottet, and G. Lockard, "Doppler lidar sensor for precision landing on the moon and mars," in *2012 IEEE Aerospace Conference*, March 2012, pp. 1–7.

[8] F. Amzajerdian, D. Pierrottet, L. Petwat, G. Hines, B. Barnes, and G. Lockard, "Fiber doppler lidar for precision navigation of space vehicles," in *Lasers, Sources, and Related Photonic Devices.* Optical Society of America, 2012, p. FTh3.1A.2. [Online]. Available: http://www.osapublishing.org/abstract.cfm?URI=FILAS-2012-FTh3.1A.2

[9] F. Amzajerdian, L. Petway, G. Hines, B. Barnes, D. Pierrottet, and G. Lockard, "Doppler lidar sensor for precision landing on the moon and mars," in *2012 IEEE Aerospace Conference*, March 2012, pp. 1–7.

[10] F. Amzajerdian, D. Pierrottet, G. D. Hines, L. Petway, and B. W. Barnes, "Coherent doppler lidar for measuring velocity and altitude of space and arial vehicles," 2016.

[11] D. Pierrottet, F. Amzajerdian, L. Petway, B. Barnes, and G. Lockard, "Flight test performance of a high precision navigation doppler lidar," in *SPIE Defense, Security, and Sensing*. International Society for Optics and Photonics, 2009, pp. 732 311–732 311.

[12] D. Pierrottet, F. Amzajerdian, L. Petway, B. Barnes, G. Lockard, and G. Hines, "Navigation doppler lidar sensor for precision altitude and vector velocity measurements: flight test results," in *SPIE Defense, Security, and Sensing*. International Society for Optics and Photonics, 2011, pp. 80 440S–80 440S.